JOURNAL OF Materials CHEMISTRY

Anomalous scattering study of oxide scales formed at 1173 K on surface modified stainless steel

M. J. Capitan,[a] S. Lefebvre,[b] A. Traverse,[b] A. Paúl[c] and J. A. Odriozola[c]

[a] *E.S.R.F. B.P. 220, 38043 Grenoble, France*
[b] *L.U.R.E. Bat. 209D Centre Universitaire Paris Sud, 91405 Orsay, France*
[c] *Instituto de Ciencia de Materiales de Sevilla and Departamento de Química Inorgánica, Centro Mixto Universidad de Sevilla-CSIC, Av. Americo Vespuccio, s/n. 41092 Sevilla, Spain*

Received 23rd March 1998, Accepted 6th July 1998

The effect of lanthanum deposits on AISI 304 grade stainless steels has been studied by anomalous scattering, X-ray diffraction, Rutherford backscattering spectrometry (RBS) and scanning electron microscopy coupled with a energy dispersive spectrometer (SEM-EDX). The lanthanum deposits were obtained by the pyrosol method which implies the interaction at 473 K of an aerosol of lanthanum nitrate with the steel surface. The deposits enhance the corrosion resistance of the stainless steels specimens under synthetic air at 1173 K by a factor of three with respect of the non-treated steels. The main crystalline component of the protective oxide scale is demonstrated to be Fe_2O_3. This result is explained on the basis of the oxide crystallinity and the chemical reactions at the alloy surface during the deposition procedure.

1 Introduction

High temperature resistant alloys have to comply with two main requirements: a low growing rate formation of a protective scale and adequate adhesion of such a layer to the alloy, especially if thermal cycles are considered. According to literature data the best suited oxides are Cr_2O_3 and Al_2O_3 since diffusion through them is relatively slow.[1–8] Thus, most of the commercially available refractory alloys (Fe–Cr, Co–Cr, Ni–Cr, Co–Cr–Al, Ni–Cr–Al, Fe–Cr–Al, ...) are either chromia- or alumina-forming alloys.

Conventional stainless steels (*e.g.* AISI 304 and AISI 316 grades) are grouped within the chromia-forming alloys. Such alloys form a Cr_2O_3 layer that protects the bulk against corrosion up to temperatures of around 900 K. Outward diffusion of cationic species and inward diffusion of oxide ions are responsible for the formation of the protective layer. As a consequence of these diffusion mechanisms, a parabolic rate law fits the oxidation process.[1] At higher temperatures, and especially when thermal cycles are used, the stresses generated in the oxide scale result in spalling with loss of chromium from the alloy which is no longer resistant to oxidation.

The beneficial effects of active element additions on the oxidation resistance of many heat resistant alloys are well known. Small amounts, usually below 1%, of reactive elements (Sc, Ti, Y, Zr, Ce, La, ...) clearly improve the oxidation behaviour of chromia- and alumina-forming alloys.[2–8] Several explanations have been given for this effect, usually termed reactive element effect (REE), among them: modification of the diffusion mechanisms, vacancies condensation, formation of reactive element oxide inclusions, formation of perovskite-type phases, ... However, no clear conclusions have been drawn for this effect.

Since the pioneering work of Pfeil[3] several methods of surface-depositing reactive elements have been proposed. For instance CVD methods,[9] electrodeposition methods,[10] ion implantation[11,12] and application of nitrate containing solutions.[6–8] Most of the proposed methods are too costly to preclude industrial applications at intermediate temperatures (1150–1350 K). In this work we propose the study of conventional stainless steels (AISI 304 grade) onto which lanthanum has been deposited by a non-costly method consisting of a modified CVD procedure.[13,14] The purpose of this work is to study possible correlation between the structure of the compounds present in the oxide scale and the REE.

The dependence of the atomic scattering factor for X-rays with the incident wavelength enables differentiation between the elements present in the oxide scale which should normally show low contrast for X-rays owing to their proximity in the periodic table (*i.e.*, iron and chromium). In this way it would be possible to elucidate some of the proposed factors for the REE: in terms of grain size of the chromia layer or formation of new phases.

2 Experimental

2.1 Sample preparation

AISI 304 grade steel specimens from Acerinox, S.A., Spain ($40 \times 20 \times 2$ mm) were polished on 1000 grit SiC paper, cleaned in ethanol, water and dried. Samples were later passivated in air for 24 h; the chemical composition is shown in Table 1.

The lanthanum deposition process was by means of the pyrosol method, a modification of CVD processes. Briefly, it consists in generating an aerosol of controlled particle size from a 0.1 M solution of lanthanum nitrate. Nitrogen is passed through this aerosol transporting aerosol particles to a furnace at 473 K where the steel specimen is placed. Decomposition of the aerosol in contact with the steel surface results in an homogeneous deposit of lanthanum oxide.[14]

Lanthanum deposition is carried out over two series of samples; air passivated AISI 304 grade stainless steels (WLA samples) and air oxidised stainless steels (PLA samples). The latter samples were prepared by heating under synthetic air to 1173 K at a heating rate of 100 K min^{-1} maintaining this temperature for 2 min before cooling to room temperature at

Table 1 Chemical composition (weight %) of the AISI 304 grade used in this study

Cr	Ni	Si	Mn	N	C	Cu
18.36	8.11	0.44	1.45	0.057	0.064	0.23
Mo	P	S	Co	V	W	Fe
0.25	0.03	0.001	0.2	0.13	0.015	Balance

80 K min^{-1}. For comparison a reference sample is also studied; AISI 304 grade steel without any lanthanum treatment.

All the samples were subjected to a final oxidation process under synthetic air at 1173 K for 480 min. The oxidation process was carried out and monitored in a thermobalance (Setaram TG92). The oxidation time was chosen in such a way that pseudoparabolic behaviour still remains for the reference sample. Longer oxidation periods result in deviations from parabolic kinetics and spalling off in the oxide scale for the untreated sample.

2.2 Characterisation methods

X-Ray experiments were carried out on a four circle goniometer set up at the D23 beam line (LURE-DCI, Orsay-France).[15] The beam line is equipped with a double crystal [Si(111)] monochromator with fixed exit and sagittal focusing; detection was *via* a NaI scintillator combined with a Ge(111) analyser. The analyser increases the angular resolution and the signal to background ratio by suppressing fluorescence. The instabilities of the incident beam are automatically corrected by a monitor detector which records diffuse scattering from a Kapton foil. The data are recorded by an angular scan in the vertical diffraction plane.

Two main properties of the synchrotron beam were essential for resolving the structural problem we were faced with: parallelism of the beam in the vertical plane and tunability of the wavelength. First, high resolution is necessary to separate diffraction lines of compounds with similar structures and very close cell parameters as, for example, series of compounds where Fe/Cr isomorphic substitutions are possible as in $Cr_{1.3}Fe_{0.7}O_3$, Fe_2O_3 and Cr_2O_3. Second, tunability gives the possibility of increasing the contrast between iron and chromium which is very weak ($\Delta Z = 2$), although it can be modified by choosing wavelengths near the absorption edges of both elements. The wavelengths were chosen 100 and 10 eV under the absorption edges of iron (1.7702 and 1.7445 Å) and 10 eV under that of chromium (2.0715 Å). These wavelengths were adjusted by reference to EXAFS spectra from Fe and Cr foils. The accuracy of energy determination is 2 eV and the wavelength resolution ($\Delta\lambda/\lambda$) is equal to 2×10^{-4} Å.

The oxide scale was also characterised by means of Rutherford back scattering (RBS) as well as scanning electron microscopy (SEM).

The RBS analysis was done in the Orsay accelerator ARAMIS[16] using 2 MeV He^{2+}. The energy of the incident beam was chosen to obtain a good separation between lanthanum and transition metals (Cr, Fe, Mn and Ni).

The instrument used for the SEM is a Zeiss DSM 950 combined with a TRACOR 5400 for the chemical analysis. This instrument does not analyse oxygen.

3 Results

3.1 Thermogravimetry

Fig. 1 shows characteristic oxidation curves obtained for each series of samples, monitored thermogravimetrically. A pseudo-parabolic behaviour according to Wagner's law[1] can be observed in each case for the first 10 h of oxidation. However, for the untreated steel, deviation from such behaviour is observed over later periods. For longer oxidation periods a combination of linear and exponential rate laws is observed for this sample. Lanthanum-coated specimens remain within the parabolic behaviour for the whole period of time sampled (up to 140 h) either for PLA or WLA samples.

Despite the shape of the curve, the mass gain per cm^2 is much lower, even in the parabolic range for the lanthanum-treated samples that are approximately three times less reactive than the untreated specimens (Fig. 1). After 8 h oxidation (chosen as oxidation time for the studied samples) the total

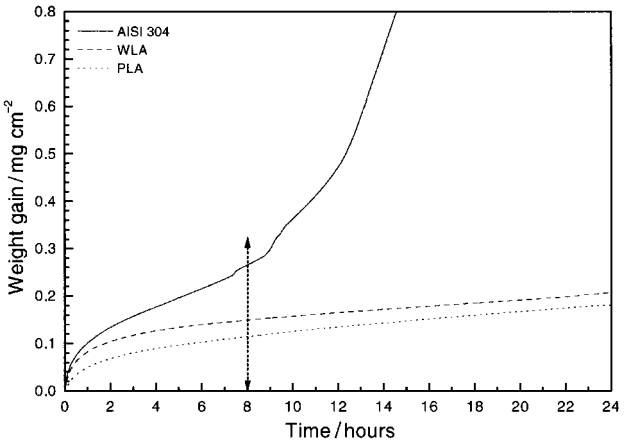

Fig. 1 Oxygen weight gain of the samples under isothermal heating in synthetic air at 1173 K for the untreated steel (AISI 304) and lanthanum deposited steels (PLA and WLA); the double ended arrow indicates the weight gain after 8 hours isothermal oxidation.

mass gain in the lanthanum-coated samples is essentially independent of the steel pretreatment. However, the initial stages of the oxidation slightly depends on pretreatment. It can be concluded from the data in Fig. 1 that pyrosol deposition of lanthanum results in an effective layer for preventing high temperature corrosion increasing the service temperature of conventional AISI 304 by around 200 K.

3.2 Scanning electron microscopy studies

The inhomogeneity of the surface and the presence of different kind of oxides appear very clearly according to SEM micrographs (Fig. 2) for the non-coated and lanthanum-coated oxidised samples. The surface aspect is completely different for both samples: the surface of the reference sample is essentially occupied by blisters mainly composed by iron and chromium, whereas these blisters are dramatically decreased (note that the scales used in both micrographs are different) and richer in iron in the La sample. Transversal cross-sections of these specimens are also shown in Fig. 2. In these cross-

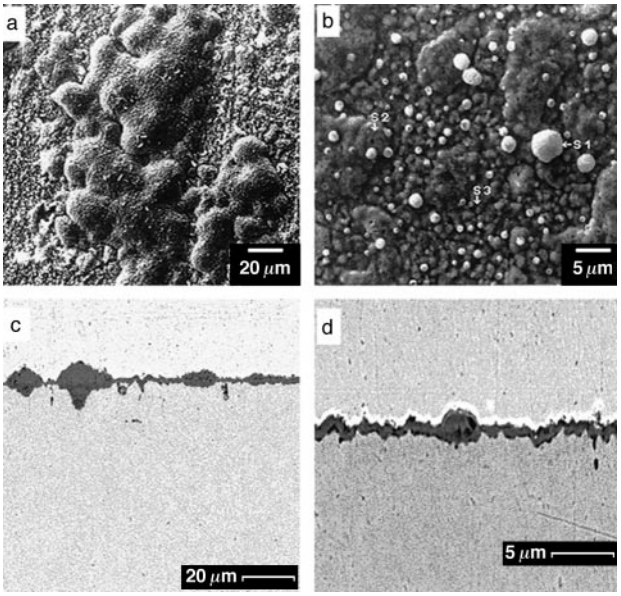

Fig. 2 SEM images of the surface of stainless steel specimens oxidised in synthetic air at 1173 K for 480 min: (a) non-treated steel, (b) lanthanum deposited steel. SEM images of cross-sections for (c) non-treated steel, (d) lanthanum deposited steel. The blister in (a) is chromium rich. The small crystals in (b) are lanthanum and chromium rich.

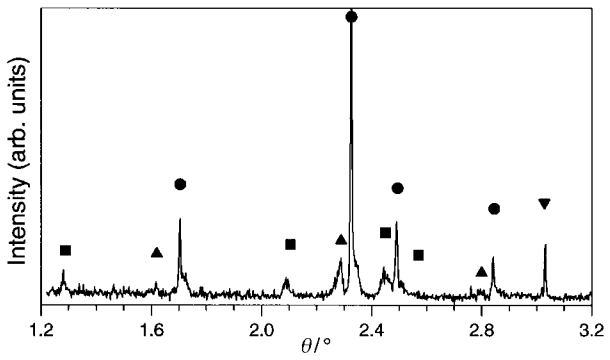

Fig. 3 X-Ray diffraction pattern for La-deposited AISI 304 oxidised for 480 min in synthetic air at 1173 K. The different families of crystalline compounds found in the oxide scale are denoted as follows: (●) M_2O_3, (■) $Mn_{3-x}M_xO_4$, (▲) $LaMO_3$ and (▼) steel.

sections the presence of nodules all over the steel surface is clearly seen in the untreated steel, with diameters of up to 5 μm, while in the La treated steel these nodules are less abundant and smaller in diameter. The presence of these blisters can be considered as a precursor to spallation. The lower content of blisters of the lanthanum treated samples shows the efficiency of the coating. In both samples the bottom is chromium and manganese rich (marked s3). Energy dispersive spectrometry (EDS) data shows that the Cr-Kα/Fe-Kα intensity ratio decreases by 30% in the lanthanum treated specimen.

In the La-coated sample [Fig. 2(b)] octahedral crystals of variable sizes (from <1 μm to a maximum of 5 μm) can be observed superimposed on plate-like particles. By fluorescence it was determined that these octahedral crystals are lanthanum and chromium rich (marked s1). It has to be considered, however, that this is not entirely conclusive since the analysed volume might be larger than the particle size.

3.3 High resolution X-ray diffraction

The X-ray diffraction pattern of a 480 min oxidised lanthanum-coated stainless steel (WLA) specimen is shown in Fig. 3. Apart from lines corresponding to the alloy structure, that can be also observed after 480 min oxidation, three different families of compounds are present. Whatever the previous lanthanum treatment of the steel surface the diffraction pattern remains unaltered. The crystalline compounds present in the oxide scale can be grouped in the following classes: M_2O_3, $Mn_{3-x}M_xO_4$ and $LaMO_3$ where M = Cr or Fe.

In all three classes of compounds a whole set of oxides with variable Cr/Fe ratio are known. These two elements may substitute each other isomorphically resulting in crystalline compounds characterised by minute changes in cell parameters.

The diffraction lines for the first class of compounds, M_2O_3, are indexed under the $R\bar{3}c$ space group with cell parameters $a=b\approx5.0$ Å, $c=13.6$ Å, $\alpha=\beta=90^\circ$ and $\gamma=120^\circ$. Table 2 lists cell parameters for Fe_2O_3, Cr_2O_3 and $Fe_{0.3}Cr_{1.7}O_3$.

The cubic phases $Mn_{3-x}M_2O_4$, having spinel structure, can be indexed in the space group *Fd*3*m* having a cell parameter of *ca.* 8.4 Å (lattice parameter values of 8.455, 8.413 and 8.499 Å are found for $Mn_{1.5}Cr_{1.5}O_4$, Mn_2CrO_4 and $MnFe_2O_4$, respectively). Tetragonal and rhombohedral distortions of this unit cell have been also reported depending on the Cr/Fe ratio.

Table 2 Cell parameters for M_2O_3 class of compounds

Compound	*a*/Å	*b*/Å	*c*/Å	JPDF file
Fe_2O_3	5.030	5.030	13.749	33-664
Cr_2O_3	4.959	4.959	13.594	38-1479
$Fe_{0.3}Cr_{1.7}O_3$	4.996	4.996	13.621	35-1112

The $LaMO_3$ compounds belong to the perovskite structural family showing a distorted cubic structure. Characteristic diffraction lines of all these compounds families are detected in the diffraction pattern of the lanthanum coated samples as shown in Fig. 3.

Two aspects should be noted: first, the lanthanum perovskite phase is evident in the oxide scale of the lanthanum treated sample without any oxidation pretreatment. Second, the diffraction lines assigned to M_2O_3 compounds are split into two components as seen in Fig. 3. The presence of two sets of peaks is even clearer when comparing the diffraction pattern characteristic of oxidised lanthanum-coated and untreated samples with those of diffraction grade Cr_2O_3 and Fe_2O_3 samples, Fig. 4. The diffraction pattern of the oxide scale formed onto the La-coated steel surface has two components for the M_2O_3 phases, a very narrow one which is close to that found in the iron oxide and a broader one at higher *q* position close to that found in the chromium oxide. For the untreated steel the narrow peaks (lower panel in Fig. 4) appear as a broad peak that shows *q* values intermediate between those found in chromium and iron oxides.

In the lanthanum-coated steel, the relative intensities of the peaks closer to the iron phase are higher than the chromium phase. It has to be considered, however, that for the wavelength employed (1.7445 Å) the intensity of pure chromium oxide is three times lower than the intensity of pure iron oxide. The presence of the iron phase is not due to any oxide spallation because the oxidation time for these samples was chosen in order to avoid this process in all the samples as is clearly shown by thermogravimetric behaviour and SEM micrographs of these samples.

The full width at half maximum of the narrow peaks is close to that found in the reference iron oxide sample which is a diffraction standard from NBS (National Bureau of Standards). Thus it can be concluded that the iron phase shows excellent crystallinity with the domain of coherence being close to 1000 Å.

In order to identify the different crystalline phases present in the oxide scale best-fit techniques have been used to calculate the cell parameters of the observed oxide phases. Table 3 lists the calculated cell parameters for the observed M_2O_3 class of compounds.

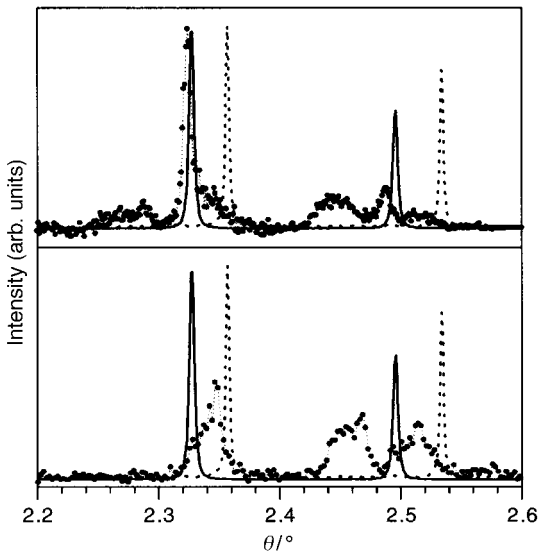

Fig. 4 X-Ray diffraction patterns for the AISI 304 steel (bottom panel) and La-coated AISI 304 (top panel) oxidised for 480 min in synthetic air at 1173 K compared with NBS diffraction standards for Cr_2O_3 (dashed line) and Fe_2O_3 (dotted line).

Table 3 Calculated cell parameters for the observed M_2O_3 class of compounds

Phase	a/Å	b/Å	c/Å	α/°	β/°	γ/°
M_2O_3-I	5.05	5.05	13.77	90	90	120
M_2O_3-II	4.99	4.99	13.65	90	90	120

Within the precision limit of the fitting technique the lattice parameter of the M_2O_3-I phase is close to that of Fe_2O_3, and that of M_2O_3-II close to Cr_2O_3 (Table 3). The relative proportion of the latter phase is higher in the oxide scale formed on the reference steel as described above [Fig. 4(b)]. For this sample only the chromium phase is clearly present.

The peak position of the lanthanum phase indicates the existence of a $LaCrO_3$ phase but the number of diffraction lines observed, only two, prevents the determination of cell parameters in a phase that can be indexed in the orthorhombic system.

$Mn_{3-x}X_xO_4$ cubic phases are fitted with a cell parameter of 8.46 Å compatible with $MnCr_2O_4$. However, a small shift of the manganese peaks is observed for the La-coated preoxidised steel (PLA). Although more experiments are needed to verify that the manganese concentration has some influence on the spalling behaviour of the oxide scale, it might be postulated that small differences between the preoxidised (PLA) and non-preoxidised (WLA) La-coated steel samples are related with the intensity increase corresponding to the presence of manganese ions.

3.4 RBS studies

In order to have an estimation of the relative proportion of iron and chromium present in the oxide scale RBS experiments with 2 MeV He^{2+} have been carried out. In agreement with the diffraction measurement almost no difference is observed between both lanthanum coated samples at the same oxidation time (480 min). Fig. 5(left) shows the spectrum obtained for the La-coated steel (WLA) after 480 min of oxidation. It was observed that the oxidation process produces a modification in the La distribution profile. Before the oxidation process the La distribution profile showed an exponential decrease from the surface towards the bulk becoming an almost linear profile in depth after 480 min of oxidation [Fig. 5(left)].

The slope of the RBS curve around the Fe–Cr signal led us to believe that the iron concentration is higher than that of chromium. This behaviour is clearly different to that previously reported by Ager *et al.*[12] where the chromium signal is more prominent than the iron signal.

Quantification of RBS spectra for such complex systems is not an easy task owing to the number of components of very similar atomic number in the target. According to the RUMP method,[17] an array of layers of variable composition containing the different elements present in the oxide scale has to be built up. According to the simulation (smooth solid lines in Fig. 5) lanthanum profiles present a more or less linear decrease on approaching the oxide/alloy interface having consequently a maximum at the oxide scale surface. It was observed that a slightly lower amount of lanthanum deposited in the preoxidised steel (PLA sample) compared to WLA. This has to be related to the deposition process that seems to be less effective over the oxide scale than over the bulk alloy.

The more interesting point is the necessity of introducing iron in the oxide scale to properly simulate the experimental spectra. The Fe/Cr ratio for the simulated layers is always >2. This result confirms X-ray diffraction and EDS data that show higher intensity for the diffraction lines corresponding to iron oxide than those corresponding to chromium oxide. If we consider the simulated atomic fraction of the topmost layers the Cr_2O_3/Fe_2O_3 ratio is equal to 0.12. Although the simulation can only be regarded as semiquantitative this result agrees fairly well with the relative intensity of the diffraction lines. Fig. 5(right) shows a tentative fit with a higher concentration of Cr at the oxide scale but the best fit obtained under this condition is poorer than with higher Fe concentration.

3.5 Anomalous scattering

The anomalous scattering process is based on the fact that the X-ray atomic diffusion factor is wavelength dependent. We express this factor as:

$$f_j = f_j' + i f_j'' = f_j^0(\sin\theta/\lambda) + \Delta f_j'(\lambda) + i\Delta f_j''(\lambda)$$

where f is the atomic scattering factor for atom j corrected for the anomalous dispersion. The real and imaginary parts of the atomic absorption factor have a sudden modification when the energy of the incident X-ray beam approaches that of the absorption edge of the j atom as shown in Fig. 6.

The imaginary part has an appreciable contribution in the higher energy side of the absorption edge (Fig. 6, dotted line),

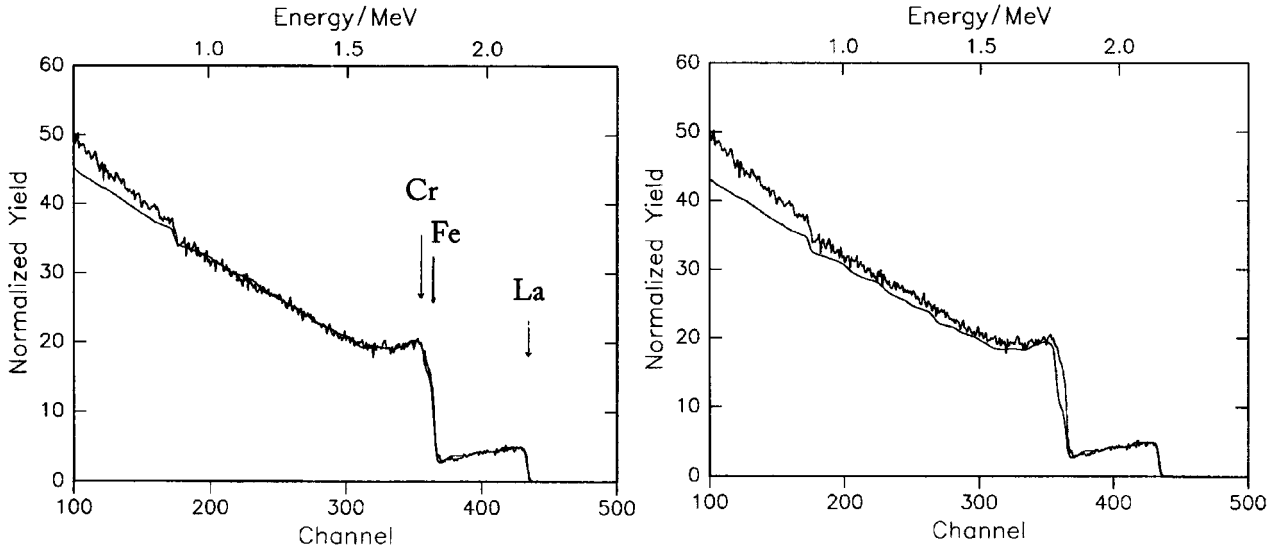

Fig. 5 RBS spectra for a La deposited specimen after oxidation at 1173 K under synthetic air using 2 MeV He^{2+} particles. Two fits of the experimental data using the RUMP method are included. The differences in the best fit between traces account for the relative proportions of Fe and Cr considered in the oxide scale. In the left-hand trace the Fe/Cr ratio is higher than in the trace on the right.

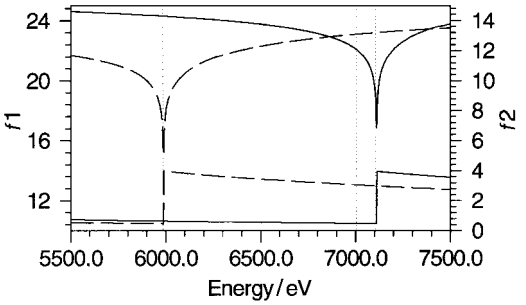

Fig. 6 Anomalous behaviour of the atomic absorption factor for X-rays near the absorption edge of chromium (dashed line) and iron atom (solid line).

Table 4 Atomic scattering factors taken from Sasaki tables ref. 18

Atom (Energy/eV)	f'	f''
Cr (5900)	19.93	0.47
Cr (5985)	17.08	0.48
Fe (7107)	18.83	0.47
Fe (7004)	22.15	0.48

and the real part has a sharp negative peak at the absorption edge (Fig. 6, solid line). If we compare the f values for Fe and Cr atoms at two different wavelengths close to their absorption edges, Table 4, it can be seen that on modifying the wavelength the intensity of the diffraction lines corresponding to planes containing the element sampled will be appreciably altered.

If experiments are carried out close to the absorption K edge of iron (7107 eV) and far from it (7004 eV) a decrease of 20% in the intensity of the diffraction lines is expected. The experimental intensity obtained for a reference iron oxide at both energies is modified according to the expected percentage. The same behaviour is also expected for Cr atoms around its absorption edge (5989 eV).

Fig. 7 shows the X-ray diffraction pattern for La-coated stainless steel taken at 7107 and 7004 eV as well as the difference between them. The difference pattern (bottom curve in Fig. 7) corresponds exactly to the diffraction diagram of α-Fe_2O_3 and an extra peak characteristic of the austenite phase of the alloy. These data clearly show that the set of narrow peaks appearing in the diffraction pattern of the oxide scale of La-coated steel corresponds to a pure highly crystalline iron oxide phase.

In the same manner, the chromium containing phases can be separated by comparison of the diffraction pattern obtained at 5985 eV near the chromium absorption edge and far away at 5900 eV. Between both energies there is a change in f' and f'' of the chromium atomic factor. Both spectra have to be corrected for an absorption coefficient which is directly dependent on f'' and a precise comparison is required to normalise the beam. For varying energies the experimental intensity for

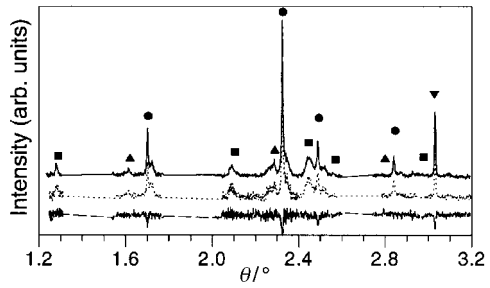

Fig. 7 The X-ray diffraction patterns for the La-coated stainless steel taken at 7107 eV (upper curve) and 7004 eV (middle curve) as well as the difference between them (bottom curve).

an infinite thickness absorption must be corrected by the mass absorption coefficient of the mixture $(\mu/\rho)_m$. It is evident that for obtaining this factor a precise knowledge of the oxide scale composition is required which is not the case here. However, a rough estimate considering the oxide scale formed by iron oxide alone may be taken into account. Even considering the simplicity of the arguments it can be concluded that the second component of the M_2O_3 phase as well as the manganese and lanthanum containing phases are mainly associated with chromium.

4 Discussion

The oxide scale thickness of the oxidised steels can be estimated assuming a homogeneous layer of M_2O_3 phases. This estimate, even though very crude, provides a reasonable approach to the oxide layer thickness by taking into account the density of the different components. The densities for Cr_2O_3 and Fe_2O_3 are 5.21 and 5.24 g cm^{-3}, respectively while for manganese containing spinels and lanthanum perovskite phases densities of 4.97 and 6.78 g cm^{-3}, respectively, can be assumed. Thus, considering that M_2O_3 phases present the more intense diffraction lines an averaged density of around 5.2 g cm^{-3} for the oxide scale seems to be reasonable. By assuming this latter value the thickness of the oxide scale is estimated from data in Fig. 1 to be 0.75 and 1.26 μm for the La-coated and untreated steel, respectively. These values are of the same magnitude to that found in previous works[7,8,12] but lower than those obtained by applying lanthanum nitrate solutions. The deposition procedure results in a similar protection against corrosion as application of lanthanum nitrate-containing solutions or ion implantation. The data suggest that the deposition procedure results in coatings as homogeneous as those prepared by ion implantation. It has to take into account, however, that the calculated thickness is smaller than that deduced from scanning electron micrographs (Fig. 2) which are 0.85 and 1.75 μm for the La-coated and the untreated steel, respectively. Values are 15 and 30% higher than those estimated by considering a dense oxide layer which indicates a higher porosity of the oxide scale in the untreated sample.

Diffraction experiments show the presence of M_2O_3, manganese- and lanthanum-containing phases. The lanthanum containing phases are mainly $LaCrO_3$ as revealed by anomalous scattering experiments at the chromium edge. This result is in accordance with the relative stability of $LaMO_3$ phases. In a previous work, it has been shown that physical mixtures of oxides containing chromium, iron and manganese result preferentially in the formation of $LaCrO_3$.[19] Thus, it can be hypothesised that lanthanum present in the oxide scale is preferentially bonded to chromium containing anions. The formation of $LaCrO_3$ crystalline phases has been previously observed.[7,8] Similarly, for yttrium implanted steels the formation of $YCrO_3$ has been reported[11] but the authors conclude the formation of such a phase scarcely influences the oxidation behaviour of the implanted steel.

The presence of iron within the oxide scale in the lanthanum-treated samples has been demonstrated by anomalous scattering experiments at the iron edge (Fig. 7). In addition to this, RUMP simulation of the RBS profiles indicate the Fe/Cr ratio within the oxide scale is up to 2 in the lanthanum treated samples (Fig. 5). This value is much lower for the non-coated steel, where the main component of the oxide scale is Cr_2O_3, which is in accordance with EDS data. This fact is surprising. It has been shown that spallation of oxide scale is related to the formation of voids where the presence of iron compounds, mainly Fe_2O_3, is evident by scanning Auger and EDS.[6] SEM micrographs of the La-deposited samples [Fig. 2(d)] indicate the absence of voids after 480 min oxidation. Moreover, the parabolic constant for the oxidation rate is even lower than that found in samples where lanthanum has been applied from

solutions.[7] These data suggest that highly crystalline Fe_2O_3, as indicated by the full width at half maximum of the diffraction lines in Fig. 4, has also a protective character as has been described for chromia or alumina scales.

It is concluded that the nature of the crystalline compounds within the oxide scale has little influence on the oxidation behaviour of the steel. The structure of lanthanum treated steel may present chromia layers as observed by applying aqueous nitrate solutions[7,8] or iron oxide layers as in this work. The important point seems to be the crystallinity of the oxide compounds present in the oxide scale. Molecular dynamics simulations on the Cr_2O_3 phase (indexed under the same space group, $R\bar{3}c$, as Fe_2O_3) clearly show that diffusion through the bulk in the absence of defects is negligible and that crystal growth is driven by the dipolar moment along the C_3 axis of the unit cell.[20] In the absence of defects and net dipolar moment of the iron oxide particle, as should be the case for oxide layers at the oxide/alloy interface, ion diffusion should be negligible considering the protective character of the oxide scale. This crystallinity has to be related to the formation of the initial oxidation layers in the nanometer range. The oxidising character of the nitrate vapours generated during the deposition process by using the pyrosol method may result in the oxidation of Cr^{3+} species to Cr^{6+} as previously stated.[19] This fact might favour the formation at the oxide/alloy interface of a continuous layer of iron oxide since this element cannot be further oxidised. By contrast, lanthanum nitrate solutions only oxidise surface layers since nitrates are only adsorbed on certain surface sites and their concentration is much lower. In order to check this hypothesis experiments are currently being carried out on the nature of the surface layers formed upon wet chemical oxidation by IR and X-ray reflectometry owing to the amorphous character and/or small crystalline domain of these layers of nanometric thickness.

5 Conclusions

Lanthanum deposition using the pyrosol method, a modified CVD procedure, is demonstrated to be very effective for protecting conventional stainless steels against high temperature corrosion (1173 K). The oxidation kinetics follows a parabolic rate law having a proportionality constant lower than that found when the refractory behaviour is attained by applying lanthanum nitrate-containing solutions to the steel surface.

X-Ray diffraction and anomalous scattering experiments show the presence of highly polycrystalline iron oxide within the oxide scale. This oxide is the main crystalline component of the oxide scales of oxidised La-treated steels. A semiquantitative approach of RBS data confirms the X-ray data.

The Fe_2O_3 layer shows a protective character against corrosion. This protective character is related to the excellent crystallinity of the oxide phase formed, similar to that found in NBS X-ray diffraction standard Fe_2O_3 samples. The formation of such a layer is a function of the deposition procedure. The oxidising NO_3^- ions present in the aerosol react at 473 K with the passive layers resulting in the formation of CrO_4^{2-}. These species favour the formation of the iron oxide layer on eliminating the Cr^{3+} of the passive film. The protective character of the Fe_2O_3 layer is explained on the basis of the similarity between its structure and that of Cr_2O_3.

We thank J. P. Dallas and J. L. Pastol of the CECM (Centre d' Etude de Chimie Metallurgique) laboratory for their help during the SEM and conventional diffraction studies. We also thank the technical staff around ARAMIS for their help during the RBS experiment. Financial support was provided by ECSC under contract MA 7210/948 and MA 7210/349 and Comision Interministerial de Ciencia y Tecnologia under contract MAT95-1093-CE.

References

1 C. Wagner, *Z. Phys. Chem. B*, 1993, **21**, 25.
2 G. R. Wallwork, *Rep. Prog. Phys.*, 1976, **39**, 401.
3 L. B. Pfeil, *U.K. Pat.*, 574088, 1947.
4 M. J. Bennet and D. P. Moon, in *The role of active elements in the oxidation behaviour of high temperature metals and alloys*, ed. E. Lang, Elsevier, Amsterdam, 1989.
5 D. P. Whittle and J. Stringer, *Philos. Trans. R. Soc., London Ser. A*, 1980, **295**, 309.
6 M. Landkof, A. V. Levy, D. H. Boone, R. Gray and E. Yaniv, *Corrosion-NACE*, 1985, **41**, 344.
7 M. I. Ruiz, J. Almagro, A. Heredia, J. Botella, J. J. Benitez and J. A. Odriozola, in *Processes and Materials. Innovation Stainless Steels*, ed. Associazione Italiana di Metalurgia, Milano, 1993, vol. 3, p. 77.
8 F. J. Ager, M. A. Respaldiza, J. C. Soares, M.F. da Silva, J. J. Benitez and J. A. Odriozola, *Acta Metall. Mater.*, 1996, **44**, 675.
9 G. Bonnet, J. P. Larpin and J. C. Colson, *Solid. State Ionics*, 1992, **51**, 11.
10 H. Konno, M. Tokita and A. Furusaki, *Electrochim. Acta*, 1992, **37**, 2421.
11 K. Przybylsk, A. J. Garrat-Reed and G. J. Yurek, *J. Electrochem. Soc.*, 1988, **135**, 509.
12 F. J. Ager, M. A. Respaldiza, A. Paul, J. A. Odriozola, C. Luna, J. Botella, J. C. Soares and M. F. da Silva, *Surface Eng. II*, in press.
13 M. B. Bemton and D. B. Swartz, *Rev. Sci. Instrum.*, 1974, **45,** 81.
14 I. Fernandez del Castillo, J. Botella and J. A. Odriozola, *Sp. Pat.*, ES P95 00709, 1995.
15 E. Elkaim, S. Lefebvre, R. Kahn, J. F. Berar, M. Lemonnier and M. Bessière, *Rev. Sci. Instrum.*, 1992, **63**, 988.
16 H. Bernas, J. Chaumont, E. Cotereau, R. Meunier, A. Traverse, C. Clerc, O. Kaitasov, F. Lalu, D. Le Du, G. Moroy and M. Salomé, *Nucl. Instrum. Methods B*, 1992, **62**, 416.
17 L. R. Doolittle, *Nucl. Instrum. Methods B*, 1985, **9,** 344.
18 Sasaki Tables National Laboratory for High Energy Physics Japan.
19 M. I. Ruiz, A. Heredia, J. Botella and J. A. Odriozola, *J. Mater. Sci.*, 1995, **30**, 5146.
20 M. A. San Miguel, L. J. Alvarez, J. Fernandez Sanz and J. A. Odriozola, *Phys. Rev. B*, submitted.

Paper 8/02233J